Modifying atomic-scale friction between two graphene sheets: A molecular-force-field study

Article *in* Physical Review B · October 2007

DOI: 10.1103/PhysRevB.76.155429

3 authors, including:

Yufeng Guo
Nanjing University of Aeronautics & Astronautics
43 PUBLICATIONS **1,196** CITATIONS

SEE PROFILE

Wanlin Guo
Nanjing University of Aeronautics & Astronautics
336 PUBLICATIONS **9,554** CITATIONS

SEE PROFILE

Modifying atomic-scale friction between two graphene sheets: A molecular-force-field study

Yufeng Guo,[1,2,*] Wanlin Guo,[2,†] and Changfeng Chen[1,‡]
[1]*Department of Physics and High Pressure Science and Engineering Center, University of Nevada, Las Vegas, Nevada 89154, USA*
[2]*Institute of Nano Science, Nanjing University of Aeronautics and Astronautics, Nanjing 210016, China*
(Received 18 June 2007; revised manuscript received 19 August 2007; published 23 October 2007)

Recently discovered ultralow friction (superlubricity) between incommensurate graphitic layers has raised great interest in understanding the interlayer interaction between graphene sheets under various physical conditions. In this work, we have studied the effects of interlayer distance change and in-sheet defects in modifying the interlayer friction in graphene sheets by extensive molecular-force-field statics calculations. The interlayer friction between graphene sheets with commensurate or incommensurate interlayer stacking increases with decreasing interlayer distance, but in the case of incommensurate stacking, ultralow friction can exist in a significantly expanded range of interlayer distance. The ultralow interlayer friction in the incommensurate stacking sheets is insensitive to the in-sheet defect of vacancy at a certain orientation. These results provide knowledge for possibly controlling friction between graphene sheets and offer insight into their applications.

DOI: 10.1103/PhysRevB.76.155429 PACS number(s): 68.35.Af, 62.20.Qp, 61.72.−y, 68.65.−k

I. INTRODUCTION

Graphite is one of the most important solid lubricants due to its weak interlayer interaction. The lubrication and friction properties of graphite have been widely investigated by friction force microscopy (FFM) techniques.[1–5] It is observed that the scanning tip of FFM performs a so-called stick-slip movement on the surface of graphite. Recently, a FFM experiment of a tungsten tip sliding on graphite revealed ultralow friction or superlubricity in the incommensurate graphene layers, and show the strong orientation dependence of the friction.[6,7] Theoretical studies based on different models have been conducted for further understanding the atomic-scale friction between finite and infinite graphene sheets.[8,9] The interlayer superlubricity state of graphite is found depending not only on the interlayer interaction but also on the pulling direction and corresponding registry of each layer. The low friction force and frictional coefficient in graphite also show dependence on loading force and interlayer stacking structures.[9] This ultralow friction behavior in incommensurate graphite may have great potential applications in miniature instruments, such as micro- and nanoelectromechanical systems.

Controlling friction and realization of superlubricity by various electronic and mechanical methods are another important issue in micro- and nanoscale devices and systems.[10–15] One recent experiment has reported that ultralow friction can be achieved by exciting the vertical mechanical resonances of a sharp silicon tip sliding on the flat surface of NaCl and KBr crystals.[10] Modulation in interaction distance and normal force therefore can significantly change the friction states. For graphite, the change of interlayer distance will undoubtedly affect the tribological behaviors of the whole system. Due to such sensitivity, understanding the effect of interlayer distance will be helpful for friction control in a graphitic system.

In reality, graphite contains different kinds of defects, such as the Stone-Wales (5-7) defect and vacancies. Those defects will change the interlayer interaction and influence the interlayer friction in graphite. However, previous theoretical and experimental studies are mainly concentrated on perfect graphene sheets without any defect.[8,9,16–19] The effects of defects in graphene sheets in modifying the interlayer friction properties remain to be explored.

The friction between graphene sheets originates from the interlayer interaction. In most previous theoretical studies, the interlayer interaction is described by a simple Lennard-Jones (LJ) type potential, which is not sensitive enough to the registry and honeycomb structures of the graphitic layers.[8,9] In this study, we employ a more accurate empirical registry-dependent potential to explore the interlayer friction properties between a graphene flake and an infinite graphene sheet. We find that the interlayer friction between graphene sheets with different registry stackings increases with decreasing interlayer distance, but the reduction in the interlayer distance between graphene sheets with incommensurate stacking has influence on the interlayer friction properties 2 orders weaker than that in the commensurate *AB* stacking system. The introduction of defects modifies the interlayer friction between the commensurate and incommensurate graphene sheets that should be considered in the modeling and interpretation of their friction behavior.

II. MODEL AND METHOD

The structural models used in our simulations are shown in Fig. 1. Here, a 190-atom rectangular graphene flake is placed onto an infinite substrate graphene sheet. The length and width of the graphene flake are 2.21 and 1.99 nm, respectively. The bilayer model is appropriate because the interaction between two nonadjacent graphene sheets is at least 50 times lower than those between two adjacent sheets.[20] We consider two representative interlayer stacking cases: (1) the graphene flake put on the substrate graphene sheet with the *AB* stacking orientation, a typical commensurate structure in graphite; and (2) the same graphene flake rotated by 90° and arranged randomly on the substrate, as shown in Fig. 1(b). The second case leads to an incommensurate stacking be-

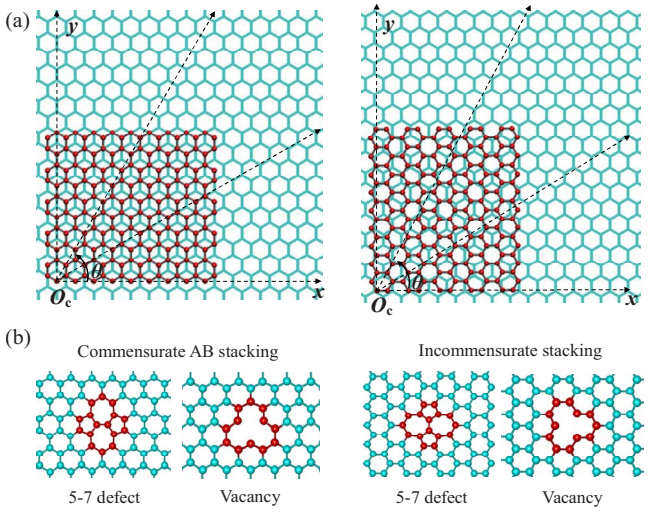

FIG. 1. (Color online) (a) A finite 190-atom rectangular graphene flake is stacked on another graphene with initial *AB* stacking (left). Then the same graphene flake is rotated by 90° and placed randomly on the substrate graphene to form an incommensurate stacking (right). The graphene flakes slide 3 nm on the lower graphene sheets along different directions θ. (b) A 5-7 defect and a vacancy created by removing one atom are introduced into the commensurate (left) and incommensurate (right) graphene flakes, respectively.

tween the graphene flake and the infinite graphene sheet. Our study is aimed at the investigation of the influence of interlayer distance and defects on the friction between these graphene sheets. We consider a 5-7 defect and a vacancy created by removing one atom in both cases, as shown in Fig. 1(b).

The interlayer interaction in the layered graphitic sheets is dominated by the long-ranged van der Waals (vdW) interaction. Large-scale simulations of nanoscale systems are beyond the capabilities of *ab initio* quantum mechanical methods such as density function technique. Therefore, empirical methods capable of predicting both the energy level and the equilibrium distance at the vdW distances are needed for studying large graphitic systems. Recently, a registry-dependent interlayer interaction potential is specifically parametrized for layered carbon structures by Kolmogorov and Crespi[21–23] (KC) or the KC potential:

$$V(\vec{r}_{ij},\vec{n}_i,\vec{n}_j) = e^{-\lambda(r_{ij}-z_0)}[C + f(\rho_{ij}) + f(\rho_{ji})] - A\left(\frac{r_{ij}}{z_0}\right)^{-6},$$

$$\rho_{ij}^2 = r_{ij}^2 - (\vec{n}_i\vec{r}_{ij})^2, \quad \rho_{ji}^2 = r_{ij}^2 - (\vec{n}_j\vec{r}_{ij})^2,$$

$$f(\rho) = e^{-(\rho/\delta)^2}\sum C_{2n}\left(\frac{\rho}{\delta}\right)^{2n}, \tag{1}$$

where $\vec{r}_{ij}$ and r_{ij} are the distance vector and the nonbonding interatomic distance, and $\vec{n}_i$, $\vec{n}_j$ are the normal vectors. The function f, which reflects the directionality of the overlap, rapidly decays with the transverse distance ρ.[21] The detailed definition of these vectors and the parameters in the above

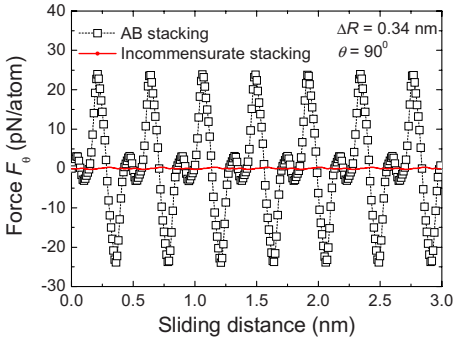

FIG. 2. (Color online) Variations of the in-plane force F_θ acting on the perfect graphene flakes in the *AB* stacking and incommensurate stacking with an interlayer distance $\Delta R = 0.34$ nm when sliding along $\theta = 90°$.

equations can be found in Ref. 21. This potential contains a vdW attraction and an exponentially decaying repulsion due to the interlayer wave-function overlap.[21] Different from the LJ potential, the KC potential is mainly determined by two parameters: $\vec{r}_{ij}$ and ρ. This setting has been proven to be more effective in describing the registry-dependent interlayer interaction of adjacent graphene layers than the LJ potential.[20–25] The interlayer force acting on the graphene flake can be expressed as

$$\vec{F} = -\sum_{i=1}^{N_f}\sum_{j=1}^{N_s}\frac{\partial V(\vec{r}_{ij},\vec{n}_i,\vec{n}_j)}{\partial \vec{r}_{ij}}, \tag{2}$$

where i denotes an atom in the graphene flake and j an atom in the substrate graphene sheet, and N_f and N_s are the numbers of atoms of the graphene flake and substrate involved in calculations, respectively. The whole structures of the perfect and defected graphene flakes are all relaxed by the total energy minimization method based on AMBER molecular force field before the statics calculations.[26] The relaxed graphene flakes are then fixed at different interlayer distances and rigidly slide on the substrate graphene sheet for 3 nm along a given orientation, and the sliding of 3 nm is repeated for each small increment of the orientation angle θ, as shown in Fig. 1. At each sliding step of 0.01 nm, the corresponding interlayer energy and interaction force F_θ acting on the graphene flake along direction θ are calculated by the KC potential.

III. RESULTS AND DISCUSSION

Figure 2 shows the variations of the in-plane force F_θ acting on the perfect graphene flakes of *AB* stacking and incommensurate stacking, with an interlayer distance of 0.34 nm when sliding along $\theta = 90°$. Here, the negative force F_θ means that the force is opposite to the sliding direction, which can be seen as the resistance or friction force. It is shown that the magnitude of force variation for the *AB* stacking is much higher than that for an incommensurate stacking. The maximum force F_θ opposite to the sliding direction or the maximum resistance force acting on the graphene flake is directly related to the interlayer static friction properties.

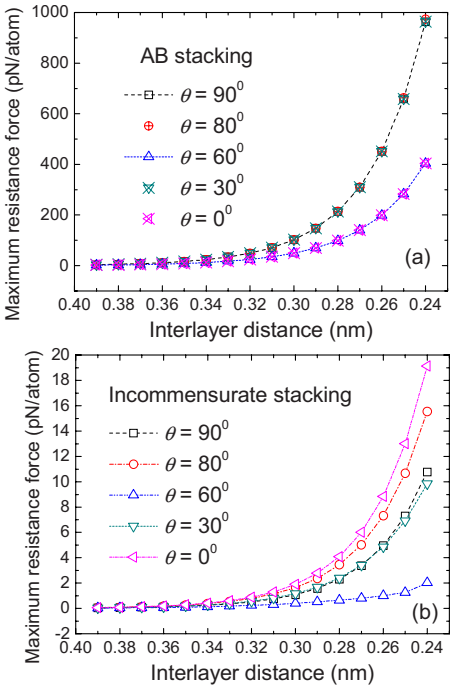

FIG. 3. (Color online) Maximum resistance force acting on the perfect graphene flakes in (a) *AB* stacking and (b) incommensurate stacking with different interlayer distances along different sliding directions θ.

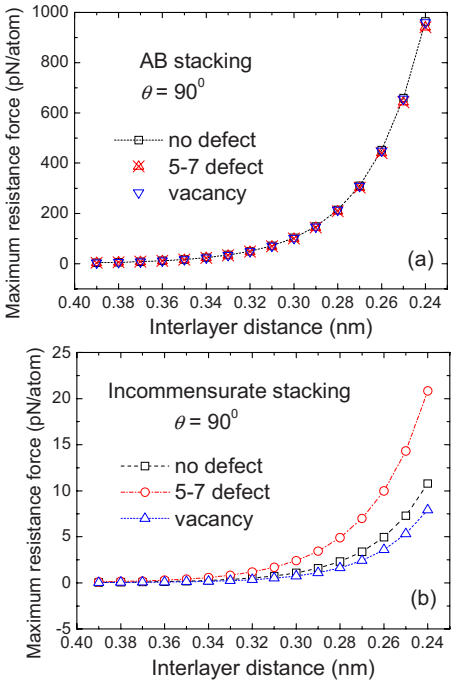

FIG. 4. (Color online) Variations of maximum resistance forces acting on the graphene flakes of different defects in (a) *AB* stacking and (b) incommensurate stacking with interlayer distance along $\theta = 90°$ direction.

Figure 3 plots the variations of maximum resistance force with interlayer distance in the *AB* commensurate and incommensurate stackings along different sliding directions. When the interlayer distance is 0.39 nm, the two graphene sheets are still bound together, but the average maximum resistance forces in the *AB* and incommensurate stacking systems are only 3 and 0.05 pN/atom. Compared to the average maximum resistance force at the interlayer distance of 0.34 nm, the small force in the *AB* stacking case suggests that the low interlayer friction can be realized in commensurate graphene sheets by increasing the interlayer distance to a suitable value. In the incommensurate stacking case, the maximum resistance force at each interlayer distance is approximately 2 orders of magnitude lower than that in the *AB* stacking case. Thus, the incommensurate graphene sheets can be considered as an interlayer superlubric system. Previous experimental and theoretical studies show that the total friction force in flat graphite for most relative orientations was lower than 50 pN (superlubricity), but for narrow ranges of orientation, the friction was as high as 250 pN.[6–8] Although the magnitude of the resistance forces in our calculations is not suitable to directly compare with the friction forces measured in experiments and calculated in other theoretical studies, the ultralow resistance force in the incommensurate stacking and high resistance force in the *AB* stacking are still consistent with those studies of superlubricity in graphite.[6–8]

The normal force acting on the graphene flakes increases with decreasing interlayer distance. This enhances the interlayer friction in both the *AB* and incommensurate stacking cases. The maximum resistance forces in these two systems increase sharply when the interlayer distance ΔR is less than 0.3 nm. The total average normal forces acting on the $\Delta R = 0.3$ nm graphene flakes for the *AB* stacking and incommensurate stacking are 2002 and 1875 nN, respectively. Along different sliding directions, the variations of the maximum resistance forces of these two systems are different, as shown in Fig. 3. The maximum resistance force variations for the *AB* stacking system fall on a smaller number of scaling curves, indicating less influence of the sliding direction on friction in the *AB* stacking system. The reduction in interlayer distance strengthens the interlayer registry effect. As a consequence, the interlayer friction in the *AB* stacking system increases much faster than that in the incommensurate stacking system. For instance, the maximum resistance force along $\theta = 90°$ in the *AB* stacking system increases from 23.9 to 963.7 pN/atom when the interlayer distance decreases from 0.34 to 0.24 nm, while the maximum resistance force in the incommensurate stacking system increases from 0.3 to 10.8 pN/atom. The calculated results show that the variation in the maximum resistance force of the incommensurate stacking system is much more sensitive to the pulling direction. At $\theta = 60°$, the friction remains ultralow even as the interlayer distance decreases to 0.24 nm, as shown in Fig. 3(b).

To investigate the effect of defects, the variations of maximum resistance forces acting on the defected graphene flakes in the *AB* stacking and incommensurate stacking systems are plotted in Fig. 4. Same as the perfect flake, the maximum resistance forces in these defected systems increase sharply when the interlayer distance ΔR is less than 0.3 nm. The corresponding total average normal forces acting on the graphene flakes with the *AB* stacking are 2004 nN for the 5-7

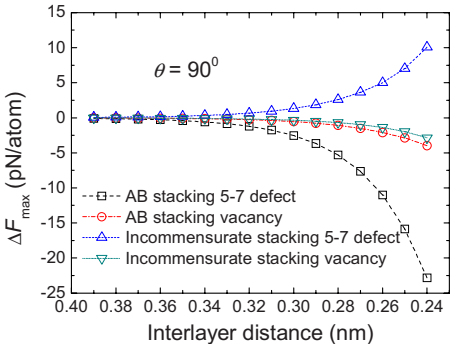

FIG. 5. (Color online) The force difference $\Delta F_{\max}$ between the maximum resistance force $F_{\max}^{defect}$ acting on the defected graphene flakes and the maximum resistance force $F_{\max}$ acting on the perfect graphene flakes along $\theta=90°$ direction; here, $\Delta F_{\max}=F_{\max}^{defect}-F_{\max}$.

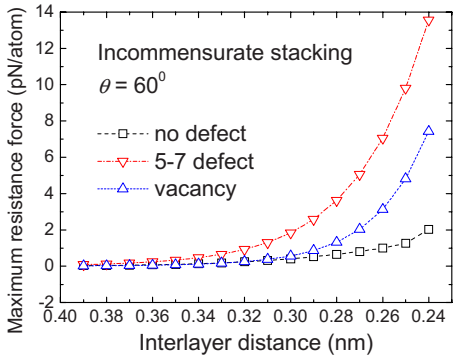

FIG. 6. (Color online) Variations of maximum resistance force acting on the graphene flakes of different defects in incommensurate stacking with interlayer distance along $\theta=60°$ direction.

defect and 2002 nN for the vacancy defect. In the incommensurate stacking, the total average normal forces acting on the $\Delta R=0.3$ nm graphene flakes are 1875 nN for the 5-7 defect and 1875 nN for the vacancy defect. Compared with the perfect graphene flake, the graphene flakes with the 5-7 defect and vacancy show small relative differences in the interlayer friction for the *AB* stacking system. In the incommensurate stacking system, these defects introduce significant relative changes to the interlayer friction properties when the interlayer distance is decreased below 0.3 nm. The friction force at the corresponding interlayer distance is increased by the 5-7 defect, but the vacancy reduces the friction force, as shown in Fig. 4(b). The lower friction in the vacancy defected flake indicates that the ultralow interlayer friction in the incommensurate stacking graphene sheets is insensitive to some types of defects at a certain orientation. A more detailed comparison between the defected and perfect graphene flakes with *AB* stacking and incommensurate stacking is given in Fig. 5. From the maximum resistance force $F_{\max}^{defect}$ acting on the defected graphene flakes and that on the perfect graphene flakes $F_{\max}$, we obtain the force difference $\Delta F_{\max}=F_{\max}^{defect}-F_{\max}$. As shown in Fig. 5, the force differences $\Delta F_{\max}$ in the defected graphene flakes with the *AB* stacking are always negative with decreasing interlayer distance. This means that both the 5-7 defect and vacancy reduce the interlayer friction in the *AB* stacking system. The 5-7 defect in the *AB* stacking graphene flake reduces the commensurate registry between the graphene sheets, as shown in Fig. 1(b), thus decreasing friction. In contrast, the 5-7 defect in the incommensurate graphene flake improves the degree of commensurate registry with respect to the substrate graphene sheet so that the interlayer friction increases.

We have also investigated the effect of sliding direction on the defected graphene flakes. In the *AB* stacking system, the effect of the defects on the interlayer friction remains the same along various sliding directions. However, the influence of defects is different in the incommensurate stacking systems when the graphene flake slides along different directions. As shown in Fig. 6, both the 5-7 defect and vacancy enhance the interlayer resistance force with decreasing interlayer distance when sliding along $\theta=60°$. This is in contrast to the case of $\theta=90°$ (see Fig. 4), where vacancy causes an opposite effect (decreasing friction). The incommensurate registry of the flake with respect to the substrate graphene is changed by the vacancy as sliding in different orientations. Therefore, the change of interlayer registry and structure induced by the defects may significantly influence the friction properties of graphene sheets with incommensurate stacking.

In our calculations, the boundaries of the 190-atom graphene flake are free. Carbon atoms on the boundaries have dangling bonds, which may affect the interlayer interaction. The number of dangling bonds depends on the size of the graphene flake. To examine the size and boundary effects, we have compared the interlayer friction of a 2.95×2.84 nm^2 350-atom rectangular graphene flake with that of the 190-atom flake. Figure 7 shows the force difference $\Delta F_{\max}$ between the maximum resistance force $F_{\max}^{350}$ acting on the 350-atom flake and $F_{\max}^{190}$ on the 190-atom flake with different defects. As shown in Fig. 7(a), there is no difference in the maximum resistance force per atom between the perfect 350-atom and 190-atom flakes in the *AB* stacking case, and the total friction force linearly increases with increasing size of the graphene flake as expected and is consistent with the previous study on the interlayer friction in commensurate graphene sheets.[8,22] The force difference $\Delta F_{\max}$ between the defected *AB* stacking 350-atom and 190-atom flakes only increases to 1.9 pN/atom even at the reduced interlayer distance of 0.24 nm. Such a small increase indicates that the change of flake size and boundary in the commensurate stacking system only has a small influence on the interlayer distance dependent static friction properties in both the perfect and defected graphene sheets. However, the change of flake size and boundary in the incommensurate stacking system introduces more pronounced changes in the interlayer static friction, as shown in Fig. 7(b). The force difference $\Delta F_{\max}$ between the 350-atom and 190-atom flakes increases sharply when the interlayer distance is reduced below 0.34 nm. In the incommensurate stacking system, the interlayer friction becomes more sensitive to the change of flake size with decreasing interlayer distance.

Moreover, we have also studied the effect of flake shape on friction by changing the rectangular flake into a hexagonal flake. It is found that the flake shape change in the *AB* stacking system does not influence the interlayer friction, but in the incommensurate stacking system, the interlayer fric-

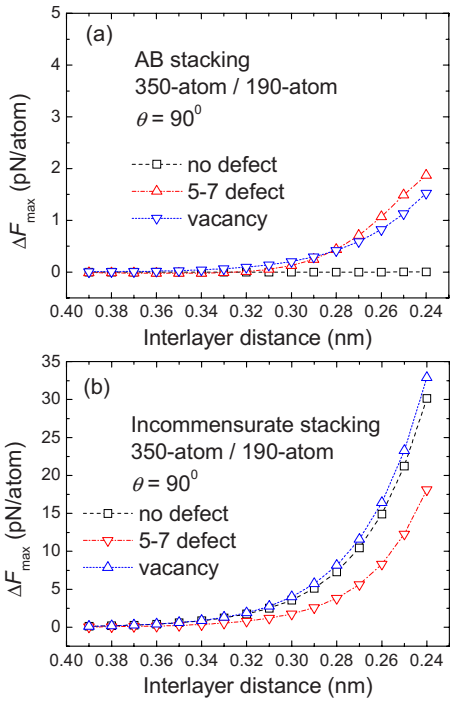

FIG. 7. (Color online) The difference $\Delta F_{\max}$ of maximum resistance force between 350-atom and 190-atom graphene flakes with different defects along θ=90° direction in (a) *AB* stacking and (b) incommensurate stacking; here, $\Delta F_{\max}=F_{\max}^{350}-F_{\max}^{190}$.

tion shows a strong dependence on the flake shape. Therefore, besides the defects, the change of flake shape and size will lead to an adjustment in the interlayer friction.

IV. CONCLUSION

We have carried out extensive molecular-force-field calculations to study the interlayer friction between graphene sheets with different interlayer stackings and defects. We have identified low static friction between graphene sheets with both commensurate and incommensurate stackings. Upon reduction of interlayer distance below the equilibrium value of 0.34 nm, the interlayer friction between the graphene sheets increases sharply with decreasing interlayer distance. Friction in the *AB* stacking graphene sheets is more sensitive to the change of interlayer distance than that in the incommensurate stacking sheets. The interlayer ultralow friction state can remain in the incommensurate stacking sheets even when the interlayer distance is reduced to 0.24 nm. Due to the change of registry, the introduction of various defects on the sheets can modify the interlayer friction properties. At a certain orientation, the interlayer ultralow friction in the incommensurate stacking sheets is found insensitive to the defect or vacancy. Our calculated results show that the change of interlayer distance and introduction of defects may provide a way to realize ultralow friction and control the friction properties in graphene sheets with commensurate and incommensurate stackings.

ACKNOWLEDGMENTS

Work at UNLV was supported by the Department of Energy Cooperative Agreement No. DE-FC52-06NA26274. This work was also supported by the 973 Program (2007CB936204), the Ministry of Education (Nos. 705021 and IRT0534), the National NSF (10732040) and Jiangsu Province NSF (Nos. BK2006185 and BK2005217) of China, and China Postdoctoral Fund (No. 20060390934).

*yfguo@nuaa.edu.cn
†wlguo@nuaa.edu.cn
‡chen@physics.unlv.edu

[1] C. M. Mate, G. M. McClelland, R. Erlandsson, and S. Chiang, Phys. Rev. Lett. **59**, 1942 (1987).
[2] J. A. Ruan and B. Bhushan, J. Mater. Res. **8**, 3019 (1993).
[3] U. D. Schwarz, O. Zwörner, P. Köster, and R. Wiesendanger, Phys. Rev. B **56**, 6987 (1997).
[4] E. Liu, B. Blanpain, J. P. Celis, and J. R. Roos, J. Appl. Phys. **84**, 4859 (1998).
[5] R. Buzio, E. Gnecco, C. Boragno, and U. Valbusa, Carbon **40**, 883 (2002).
[6] M. Dienwiebel, G. S. Verhoeven, N. Pradeep, J. W. M. Frenken, J. A. Heimberg, and H. W. Zandbergen, Phys. Rev. Lett. **92**, 126101 (2004).
[7] M. Dienwiebel, N. Pradeep, G. S. Verhoeven, H. W. Zandbergen, and J. W. M. Frenken, Surf. Sci. **576**, 197 (2005).
[8] G. S. Verhoeven, M. Dienwiebel, and J. W. M. Frenken, Phys. Rev. B **70**, 165418 (2004).
[9] K. Matsushita, H. Matsukawa, and N. Sasaki, Solid State Commun. **136**, 51 (2005).
[10] A. Socoliuc, E. Gnecco, S. Maier, O. Pfeiffer, A. Baratoff, R. Bennewitz, and E. Meyer, Science **313**, 207 (2006).
[11] J. Y. Park, D. F. Ogletree, P. A. Thiel, and M. Salmeron, Science **313**, 186 (2006).
[12] R. W. Carpick, Science **313**, 184 (2006).
[13] J. Frenken, Nat. Nanotechnol. **1**, 20 (2006).
[14] S. Y. Krylov, K. B. Jinesh, H. Valk, M. Dienwiebel, and J. W. M. Frenken, Phys. Rev. E **71**, 065101(R) (2005).
[15] A. Socoliuc, R. Bennewitz, E. Gnecco, and E. Meyer, Phys. Rev. Lett. **92**, 134301 (2004).
[16] G. A. Tomlinson, Philos. Mag. **7**, 905 (1929).
[17] H. Hölscher, U. D. Schwarz, O. Zwörner, and R. Wiesendanger, Phys. Rev. B **57**, 2477 (1998).
[18] N. Sasaki, K. Kobayashi, and M. Tsukada, Phys. Rev. B **54**, 2138 (1996).
[19] N. Sasaki, M. Tsukada, S. Fujisawa, Y. Sugawara, S. Morita, and K. Kobayashi, Phys. Rev. B **57**, 3785 (1998).
[20] W. L. Guo and Y. F. Guo, J. Am. Chem. Soc. **129**, 2730 (2007).
[21] A. N. Kolmogorov and V. H. Crespi, Phys. Rev. B **71**, 235415 (2005).
[22] A. N. Kolmogorov and V. H. Crespi, Phys. Rev. Lett. **85**, 4727 (2000).
[23] A. N. Kolmogorov, V. H. Crespi, M. H. Schleier-Smith, and J. C. Ellenbogen, Phys. Rev. Lett. **92**, 085503 (2004).
[24] G. Zhang, X. Bai, E. Wang, Y. Guo, and W. Guo, Phys. Rev. B **71**, 113411 (2005).
[25] W. L. Guo and H. J. Gao, Comput. Model. Eng. Sci. **7**, 19 (2004).
[26] The current force field procedure and parameters are available from the AMBER web site: http://amber.scripps.edu//#ff